REPORT DOCUMENTATION PAGE

Form Approved
OMB No. 0704-0188

1. REPORT DATE *(DD-MM-YYYY)*	2. REPORT TYPE	3. DATES COVERED *(From - To)*
2006	Conference Paper PREPRINT	2005

4. TITLE AND SUBTITLE	5a. CONTRACT NUMBER
Atmospheric and Platform Jitter Effects on Laser Acquisition Patterns (PREPRINT)	
	5b. GRANT NUMBER
	5c. PROGRAM ELEMENT NUMBER

6. AUTHOR(S)	5d. PROJECT NUMBER
Charles W. Hindman, Brian S. Engberg	
	5e. TASK NUMBER
	5f. WORK UNIT NUMBER

7. PERFORMING ORGANIZATION NAME(S) AND ADDRESS(ES) AND ADDRESS(ES)	8. PERFORMING ORGANIZATION REPORT NUMBER
Air Force Research Laboratory Space Vehicles 3550 Aberdeen Ave SE Kirtland AFB, NM 87117-5776	AFRL-VS-PS-TP-2006-1003

9. SPONSORING / MONITORING AGENCY NAME(S) AND ADDRESS(ES)	10. SPONSOR/MONITOR'S ACRONYM(S)
	11. SPONSOR/MONITOR'S REPORT NUMBER(S)

12. DISTRIBUTION / AVAILABILITY STATEMENT

Approved for public release; distribution is unlimited. (VS06-0016)

13. SUPPLEMENTARY NOTES
Submitted to IEEE Aerospace Conference, 4-11 Mar 06, Big Sky, MT

14. ABSTRACT

Several applications exist that require the acquisition of a distant target by illuminating it with a laser source, either cooperatively or non-cooperatively. Because of the uncertainties that exist in the knowledge of the target's position as well as the transmitting vehicles attitude, this acquisition process often involves scanning a laser beam over some uncertainty cone. The parameters of this scan can be adjusted to provide an acceptable intensity pattern within the uncertainty region. However, disturbances in the form of uncompensated platform jitter, atmospheric scintillation, and aero-optical effects due to boundary layer turbulence (if the transmitting terminal is located on a moving platform) combine to distort the desired pattern in the far field. A detailed simulation of the first two of these processes is developed and used as the basis for a trade study to show how to optimize the search parameters and maximize the probability of detection for a given set of disturbance inputs.

15. SUBJECT TERMS
Space Vehicles, Acquisition Patterns, Laser Acquisition, Search Parameters, Disturbance

16. SECURITY CLASSIFICATION OF:			17. LIMITATION OF ABSTRACT	18. NUMBER OF PAGES	19a. NAME OF RESPONSIBLE PERSON Charles W. Hindman
a. REPORT Unclassified	**b. ABSTRACT** Unclassified	**c. THIS PAGE** Unclassified	Unlimited	9	**19b. TELEPHONE NUMBER** *(include area code)* 505-853-4746

Standard Form 298 (Rev. 8-98)
Prescribed by ANSI Std. 239.18

Atmospheric and Platform Jitter Effects on Laser Acquisition Patterns

Charles W. Hindman and Brian S. Engberg
Air Force Research Laboratory
3550 Aberdeen Ave SE
Kirtland AFB, NM 87117
505-853-4746
charles.hindman@kirtland.af.mil
brian.engberg@kirtland.af.mil

Abstract—Several applications exist that require the acquisition of a distant target by illuminating it with a laser source, either cooperatively or non-cooperatively. Because of the uncertainties that exist in the knowledge of the target's position as well as the transmitting vehicles attitude, this acquisition process often involves scanning a laser beam over some uncertainty cone. The parameters of this scan can be adjusted to provide an acceptable intensity pattern within the uncertainty region. However, disturbances in the form of uncompensated platform jitter, atmospheric scintillation, and aero-optical effects due to boundary layer turbulence (if the transmitting terminal is located on a moving platform) combine to distort the desired pattern in the far field. A detailed simulation of the first two of these processes is developed and used as the basis for a trade study to show how to optimize the search parameters and maximize the probability of detection for a given set of disturbance inputs.[1][2]

TABLE OF CONTENTS

1. INTRODUCTION

Advances and use of laser and optical technology in recent years in such fields as LIDAR, Laser communications, and target tracking systems have created the need to understand and optimize the laser acquisition process.

Several experimental satellite lasercom systems have been flown or developed, including the ESA's SILEX [1,2] flight experiment, the JAXA's OICETS [3] program, and the DOD's TSAT program [4].

---

[1] U.S. Government work not protected by U.S. copyright
[2] 1595/2

2. ACQUISITION

Establishing a laser link between two platforms requires an acquisition process to enable the searching terminal to find and lock onto the other with a very small divergence beam (1 to 100s of μrads, depending on range and aperture sizes). This process can be non-cooperative, as in a target seeking search laser, or cooperative, as in a laser communications process. The initial step of this acquisition process involves a terminal scanning an illumination beam towards its target while (if applicable) trying to detect and discern the incoming optical signal in the presence of platform vibrations, cluttered optical backgrounds, and other disturbances. This initial step of scan and detect can be the most difficult and time consuming step in the process of setting up a laser lock, especially when the system is subjected to the disturbances imposed by a moving platform, atmospheric scintillation, and boundary layer effects. Previous studies have examined the impact of these disturbances on the communications link [5,6], but these studies did not include a detailed computational simulation of their effects on the acquisition process.

The small beam divergences involved in long range laser acquisition and tracking systems require precise pointing knowledge and control to be achieved. There are multiple error sources that arise to make this task more difficult, and include position, attitude, alignment, vibration, and target leading errors. These errors (described in detail below) combine to form a 'search cone' of uncertainty in which the target could appear with respect to the transmitting terminal. The acquisition process therefore involves searching out this search cone with a search laser and looking for a return signal.

Position error refers to the error in the knowledge of where the target is with respect to the transmitter. Position error is in turn composed of elements such as target ephemeris or predicted location accuracy, onboard GPS accuracy, and communication errors. Attitude accuracy depends only on how well the transmitting terminal's onboard navigation unit can measure and report the aircraft's attitude. This information must then be propagated to the aircraft, and calibration and differential motion effects introduce what we are referring to as alignment errors. Vibration errors are

caused by the motion of the aircraft that are either too fast or too large for the pointing control system to accommodate; additional errors are introduced via the actuators that are attempting to control the pointing. Note that this error can typically be greatly reduced once an optical reference signal is available to track instead of relying on the aircrafts INU. The final error to consider is that caused by differential tangential motion between the two platforms, often referred to as 'point-ahead' or leading the target. For fast and/or highly maneuverable targets, this can introduce a not insignificant additional error.
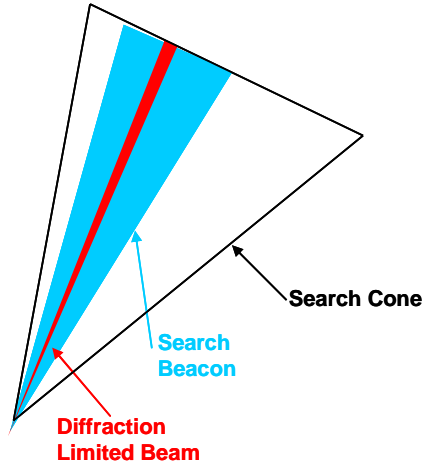

Figure 1: Search Beam Schematic

Once the search cone has been determined, the next step is to scan the laser over the search cone. Several different scanning techniques are available. For shorter ranges or smaller search cones, it may be feasible to completely fill the cone with a broadened search beam. In other instances, this might not provide enough power to establish an acquisition and a search pattern with a smaller divergence beam must be used (see Figure 1). In these cases, there are several different search patterns that are available, some of which are shown in Figure 2:
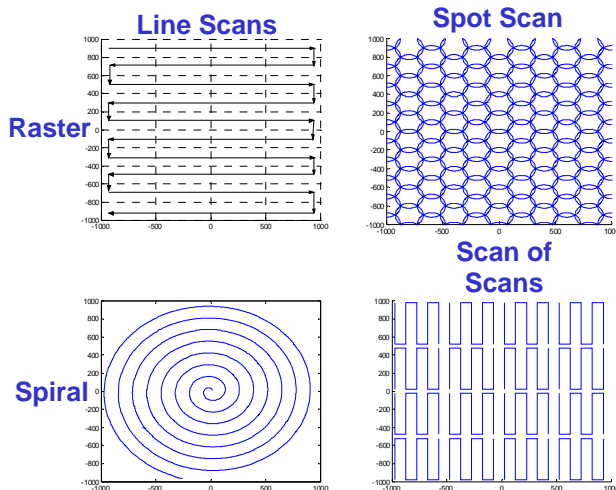

Figure 2: Search Scan Patterns

3. JITTER MODELING

Optical communications payloads on an aircraft are subject to the severe jitter vibration environment caused by engine noise, aircraft maneuvers, aeroelastic effects, etc. In the design process, the actual or expected vibration spectrum for the platform the lasercom payload is destined for should be used. Unfortunately, while vibration PSDs for a wide range of platforms are readily availably (see for example [7,8]), this data is typically only for translational rotations. Converting this data to rotational data requires making several assumptions on translating and applying the data at a new position, and is problematic at best. Additionally, no optical payload would be designed without some sort of active or passive isolation system, the effects of which must also be incorporated. For the purposes of this paper, a typical aircraft vibration environment was assumed, with the PSD shown in the top half of Figure 3:
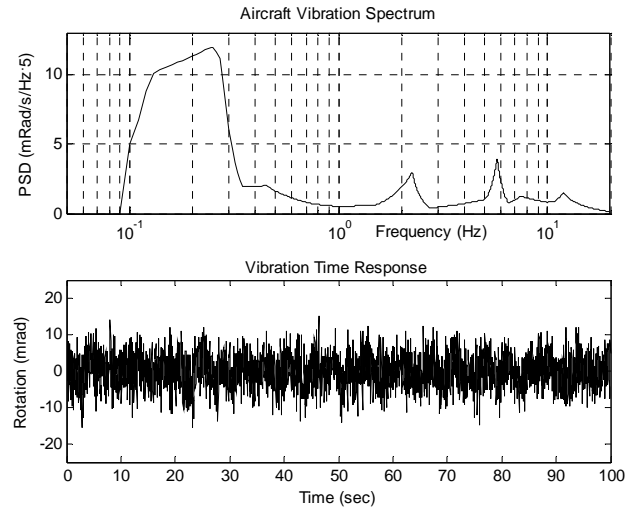

Figure 3: Aircraft PSD and Time History

A time history was created from this PSD by applying an appropriately weighted inverse Fourier transform to the PSD, with a random phase assigned to each frequency, as shown in the bottom half of Figure 3. Both X and Y time histories were created $(V_x(t), V_y(t))$, and were uncorrelated when used in the simulations later in the paper. A 30 dB broadband isolator was assumed for the simulations as well (i.e., the levels were reduced by 1000x).

4. FADE MODELING

A fade model using wave optics simulations as described in [9] was used to generate a time history F(t) of instantaneous power levels as seen by a satellite from a transmitting aircraft. The results are shown in Figure 4 for the case of an aircraft at 12200 m altitude, positioned at 36° W, 65° N, looking towards a geostationary satellite at 0° W, 0° N and an altitude of 35.6E6 m. Because of computational limitations, only 3 s of data was generated at a sampling rate of 66 μsec; for the purposes of this study this data was then

looped to form longer time histories as required. A more accurate approach would be to derive the statistical distribution from the existing data and use this distribution to generate more data.
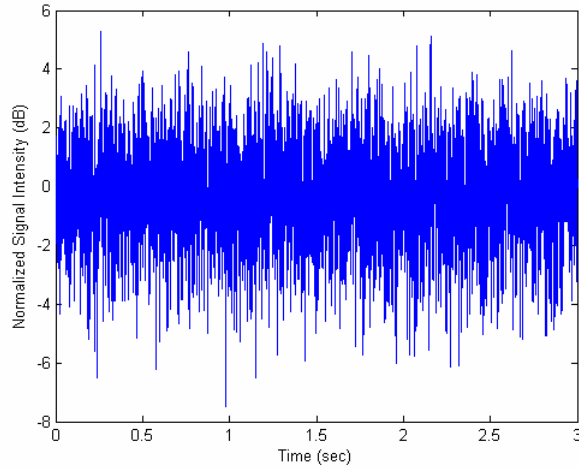

Figure 4: On-axis Fade Intensity

The simulated results as shown in Figure 4 exhibit significant variations up to a kHz or so in frequency. When this is considered in the context of an acquisition system, the effect of the integration time of the detector must come into play. Long integration times will tend to 'smooth out' the fades, as the overall process is a zero-mean one (absorption effects have been ignored). For the raw data, there is a minimum of -7.5 dB and a standard deviation of 1.6 dB.

Figure 5 shows the effect of an integration period of 0.04 sec (25 Hz rate). The maximum fade has dropped to only -0.87 dB, and the standard deviation has decreased to only 0.3 dB. Clearly most of the deleterious effects of the fading channel have been averaged over by using this integration period. However, other system considerations might come into play (very bright background levels, for example) that might force the designer to consider longer integration periods.
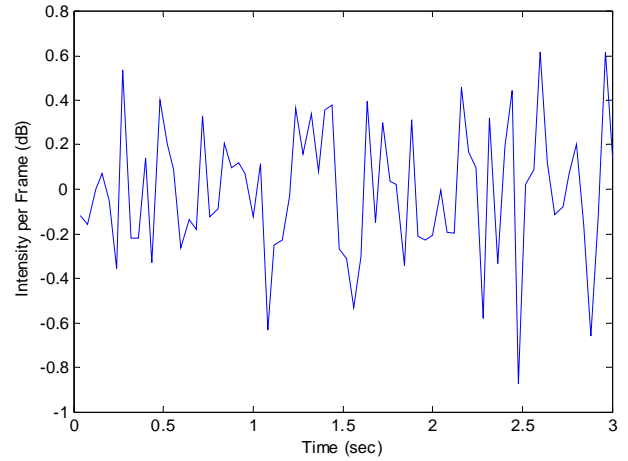

Figure 5: Fade Levels, 25 Hz Rate

When the integration period is reduced to 0.01 seconds, as shown   in
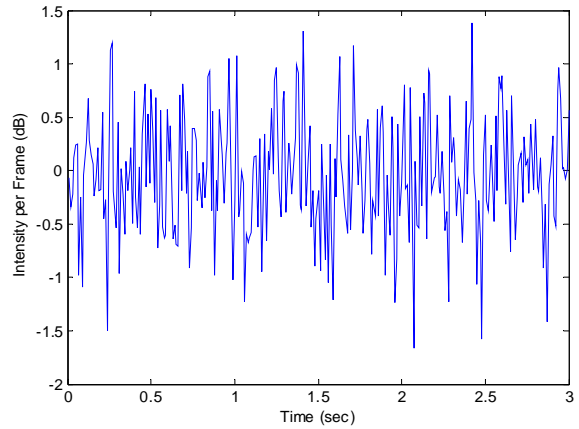

Figure 6, the fading effects are basically doubled (minimum of -1.66 dB, standard deviation of 0.55 dB), although they are still at a relatively low level .
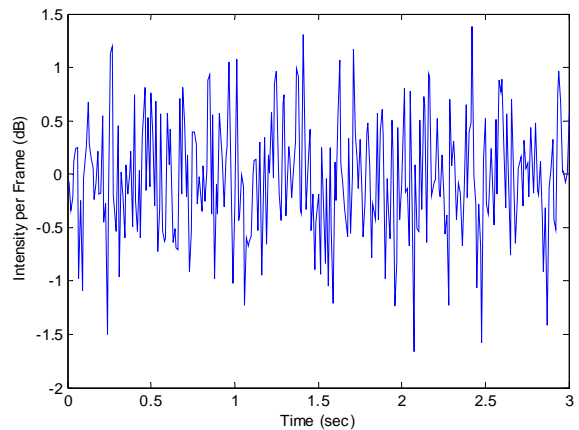

Figure 6: Fade Levels, 100 Hz Rate

Table 1 shows the minimum and standard deviation of fading losses for several different integration periods up to 1 kHz; note the significant rise when going from 100 to 500

Hz. The final entry in the table is for the raw data; most of the additional increase occurs by the 2 kHz point.

Int. Period (s/Hz)	Max. Fade (dB)	Standard Dev. (dB)
0.04 / 25	-0.87	0.30
0.02 / 50	-1.10	0.41
0.01 / 100	-1.66	0.55
0.002 / 500	-4.22	1.14
0.001 / 1000	-5.60	1.40
66E-6 / 15000	-7.49	1.62

Table 1: Fade Levels vs Integration Time

5. ACQUISITION SCAN ANALYSIS

An analysis was performed to determine the delivered energy on-orbit from a scanning aircraft. A constant linear velocity spiral scan as shown in Figure 2 was used, as described by the following set of equations (from [10]):

$$V_r = \sqrt{\frac{R_{max}\left(\frac{\theta_{1/e}}{t}\right)}{2\pi N T_{dwell}}}$$

$$V_\theta = \sqrt{\frac{2\pi N \theta_{1/e}}{R_{max} t T_{dwell}}} \quad (1)$$

$$X = V_r t \cos(V_\theta t)$$

$$Y = V_r t \sin(V_\theta t)$$

With:

$$N = \frac{R_{max} - \frac{\theta_{1/e}}{2}}{(1 - F_o)\theta_{1/e}} \quad (2)$$

Where:

V_r - Radial Velocity
V_θ- Angular Velocity
R_{max} – Maximum angular displacement (search radius)
$\theta_{1/e}$ – 1/e laser divergence beamwidth
N – Number of rings
T_{dwell} – Laser dwell time
t – Time
X – Spot X-coordinate
Y – Spot Y-coordinate
F_o – Beam overlap factor

The total time for the scan can be determined from:

$$T_{scan} = \frac{2\pi N T_{dwell} R}{\theta_{1/e}} = \frac{2\pi T_{dwell}}{1 - F_o}\left[\left(\frac{R_{max}}{\theta_{1/e}}\right)^2 - \frac{1}{2}\left(\frac{R_{max}}{\theta_{1/e}}\right)\right] \quad (3)$$

The far-field intensity was then calculated by using:

$$I(\theta, R) = \frac{\pi P D_t^2}{4\lambda^2 R^2} \exp^{\frac{-\theta^2}{2\sigma^2}} \quad (4)$$

where

$$\sigma = \frac{\sqrt{2}\lambda}{\pi D_t} \quad (5)$$

with the variables defined to be:
R – Distance (m)
θ - Off axis angle (radians)
P – Beam power (W)
D_t – Transmitting optical effective aperture
λ - Wavelength (m)

The effective aperture D_t and the 1/e beam divergence $\theta_{1/e}$ are related by:

$$\theta_{1/e} = \frac{4\lambda}{\pi D} \quad (6)$$

The far-field uncertainty region was then discretized into 1-μradian squares and the total energy intensity delivered to each square was calculated by integrating Equation (4) in time based on the laser search path developed in Equation (1), with:

$$\theta(t) = \sqrt{(X(t) - x_i)^2 + (Y(t) - y_j)^2} \quad (7)$$

where x_i, y_j is the center position of the (i,j)th square.

An example of the results from the total energy intensity calculation for a search cone of radius 200 μrads is shown in Figure 7 with no jitter or atmospheric disturbances present. Note that in this particular case, the delivered far field energy in nearly uniform, with only small ripples due to the Gaussian beam shapes.
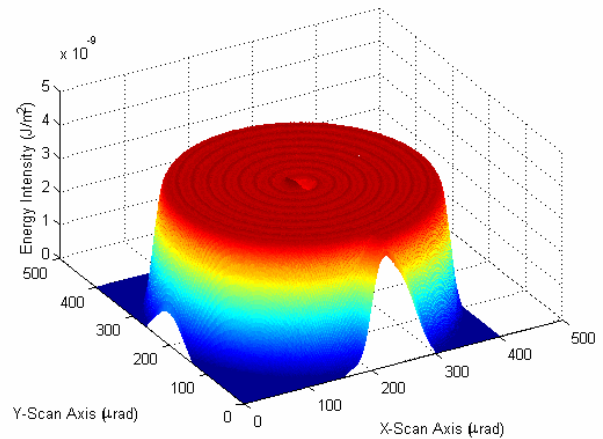

Figure 7: Far-Field Energy Density

Platform jitter is added to the simulation by modifying

Equation 7 as follows:

$$\theta(t) = \sqrt{(X(t) + V_x(t) - x_i)^2 + (Y(t) + V_y(t) - y_j)^2} \quad (8)$$

For platforms with a harsh jitter environment, the nice search patterns as seen in Figure 2 can become significantly degraded. Figure 8 shows this for the spiral search case with an vibration level of -20 dB that shown in Figure 3; note the significant holes present in the search pattern. See [11] for a more complete treatment of the effects of vibrations alone on acquisition pattern design.
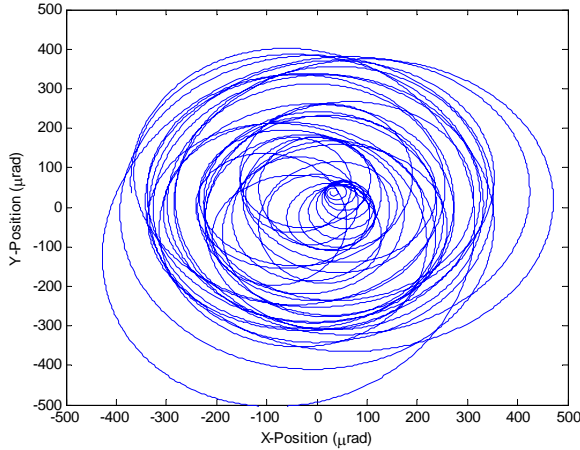

Figure 8: Spiral Search w/ Vibrations

After including the vibrations, the fade levels F(t) are added to the simulation by multiplying the fade levels with the intensity I(θ,R) from Equation 6.

Finally, the integration time effects discussed in Section 4 were included in the simulation by determining when energy falls within each search area pixel and only recording the maximum energy that falls within 1 integration period.

6. RESULTS

A nominal set of acquisition parameters was developed to produce a baseline result, shown in Table 2:

Parameter	Value
Scan Radius	200 μrad
Scan Time	1 sec
Laser Power	1 W
Beam Divergence	20 μrad (1/e dia)
Range	40,000 km

Table 2: Simulation Nominal Parameters

The initial result with no jitter or atmospheric fading for this set of parameters is shown in Figure 7; the average energy intensity in the search region is ~3.8 nJ/m^2. If the effect of atmospheric fading is then added, the results shown in Figure 9 are produced; notice how the flat-top profile that

occurs when no fading is present is replaced by the whipped meringue-type surface seen in Figure 9, with numerous peaks and valleys present.
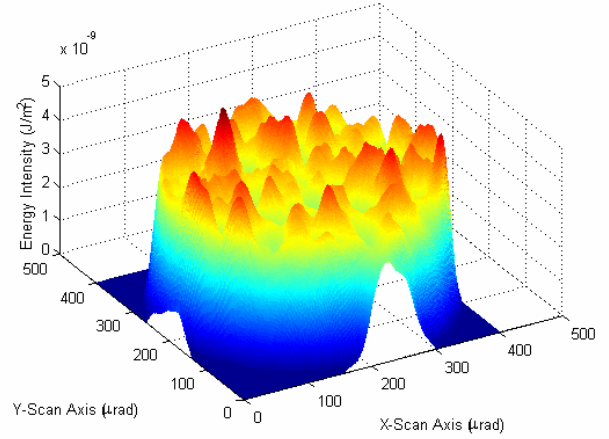

Figure 9: Fade Only Results

The natural question that then arises when examining a plot such as Figure 9 is how to derive a meaningful metric from the energy density plot. One such approach is to set a threshold energy density level and then measure the percentage of the coverage area wherein the threshold level is exceeded. This coverage statistic can then be combined with other system level specifications (such as required success rate, required probability of false alarm rate, etc) and used in the system design process.

The search area percent coverage measure is shown in Figure 10 for the case discussed above. The x-axis of this plot shows the threshold level as a percentage of the nominal average value for the case when no atmospheric fading is present (3.8 nJ/m^2). In this case, a threshold set to 55% of the no-fade average removes essentially all of the lost coverage area caused by atmospheric effects.
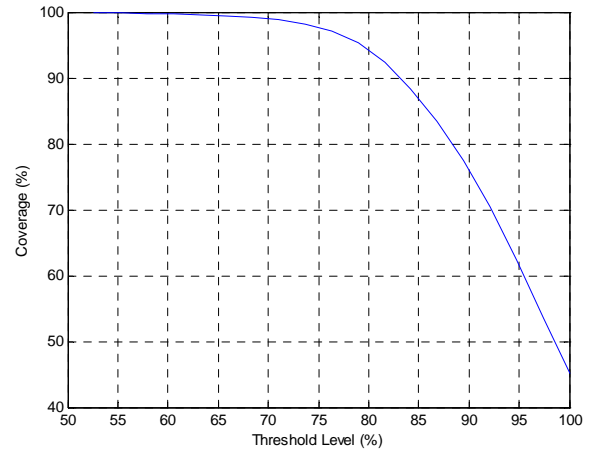

Figure 10: Coverage vs Threshold Level

Once this type of simulation tool has been developed, it becomes possible to perform trade studies to measure the

effects of fading by varying different acquisition parameters. Figure 11 shows the percent coverage measures as the beam diameter and scan time are varied. Beam diameters of 10, 20 and 40 µradians were examined as well as scan times of 1 and 3 second. Interestingly, all four cases examined exhibit virtually the same threshold level required to achieve 100% coverage (at about 55%). However, the behavior at higher threshold levels does differ considerably and some trends can be noted: As the laser beamwidth and/or scan time increases, the coverage percentage generally increases. Additionally, it should be noted that the threshold levels for the 3-second case were set to 1/3 of the level of the other cases due to 3x the energy being deposited.
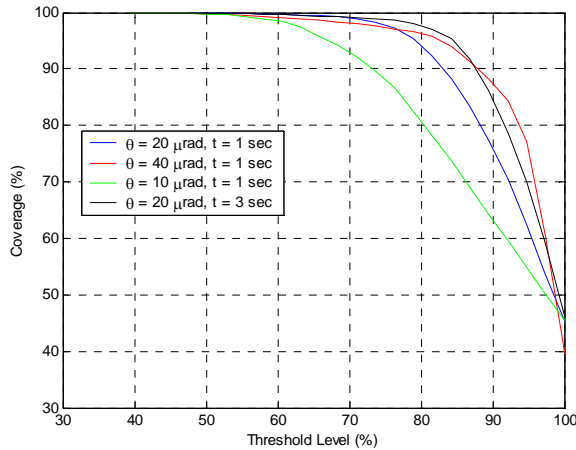

Figure 11: Fade-only Trade Study

The next step in the simulation is to combine the jitter effects as seen in Figure 3 and Figure 8 with the atmospheric fade effects discussed above. A vibration level 30 dB below that shown in Figure 3 was used along with the nominal parameters listed in

Table 2; the results are shown below in Figure 12. The vibrations have effectively damped out some of the smaller scale structure atmospheric variations and increased the large scale structural effects.
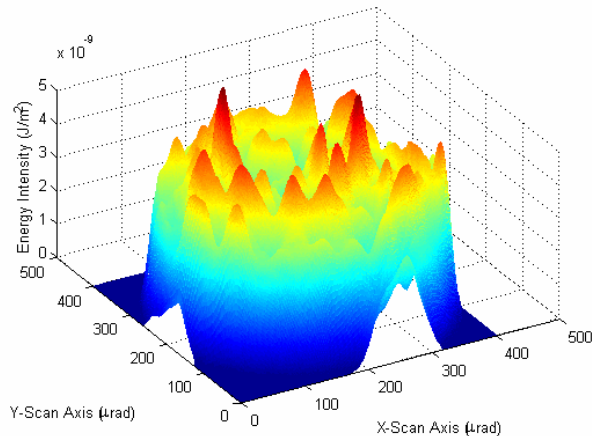

Figure 12: Fade + Jitter Results

It then becomes easy to perform multiple runs using different acquisition parameters to perform a simple trade study to consider the effects of vibrations. The results of this study for percent coverage are shown in Figure 13. In this case, the minimum threshold level to achieve 100% coverage is much lower than the fade-only case, dropping down to approximately the 10% level for the smallest (10 µrad) beamwidth. The other cases also had significant drops of 20-25% as well, and the lines are all well below those shown in the fade-only results. The overall trend that increasing the beamwidth increases the coverage percentage remained the same as before, but increasing the scan time had very little effect.
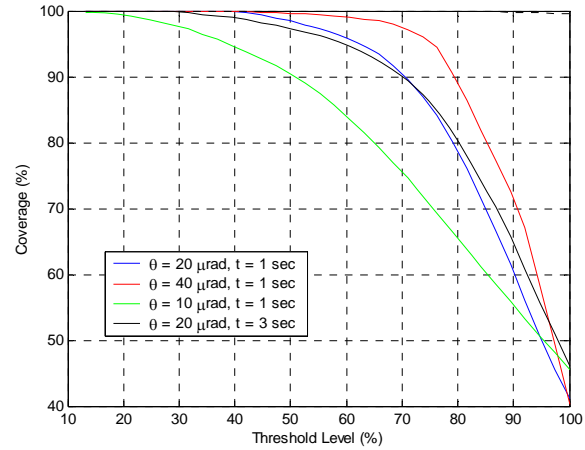

Figure 13: Fade + Jitter Trade Study

Finally, we add in the effect of finite integration times to the simulation by calculating the energy input to a given pixel of the search area within each integration period and keeping the maximum value. This produces significantly different results from before, as much of the energy gain from overlapping paths and jitter effects takes place within different integration time periods. REF shows the results for this simulation using the parameters from Table 2 with an integration time of 0.01 seconds (100 Hz frame rate). Note how the finite integration time has lowered the overall level and produced a finer spatial-scale structure than the results shown in Figure 12.
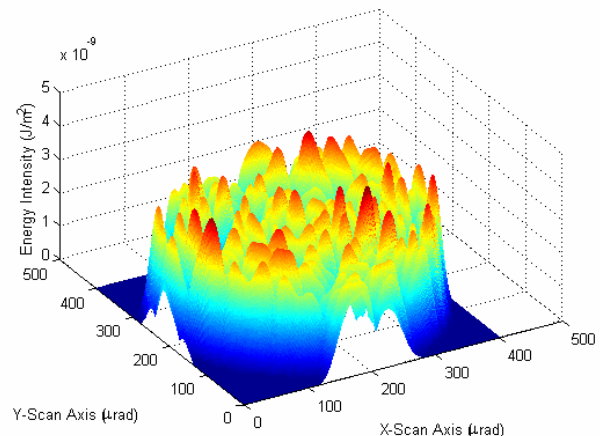
Figure 14: Integration Time Results

Performing a trade study on multiple acquisition parameters as discussed previously yields the results shown in Figure 15; an additional run with an integration time of 0.05 seconds is also included. The introduction of integration times has completely changed the relationships between acquisition parameters and coverage that existed before. For example, examine the three curves for 10, 20 and 40 μradian beamwidths with all other factors constant. Instead of increasing the coverage with increasing beamwidth as before, the 40 μradian beam has the worst coverage of the three, going to 0% coverage at threshold levels above ~55%.
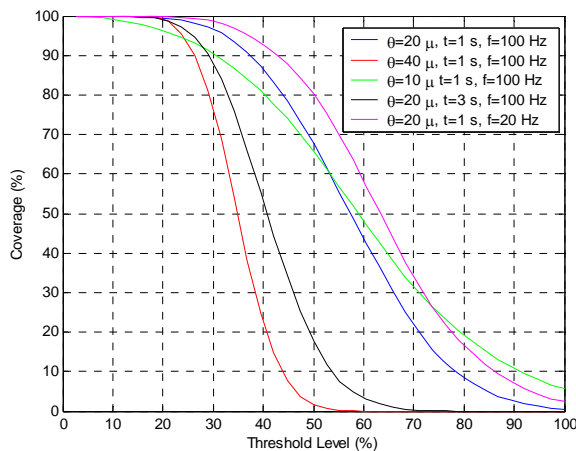

Figure 15: Integration Time Trade Study

Other important trends can also be gleaned from Figure 15. Increasing the integration time from 0.01 to 0.05 seconds did provide a slight increase in coverage; this is expected, as the previous results are valid for an effectively infinite integration time. Finally, increasing the scan time from 1 to 3 seconds gave a net decrease in coverage (whereas before it was basically a wash). One possible explanation is that the additional smearing and path crossings caused by the additional jitter in the three second scan are no longer captured because they fall outside of a single integration period.

7. CONCLUSIONS

A detailed simulation of the deposited far-field energy from an acquisition scan in the presence of onboard jitter and atmospheric fading effect was developed. Exercising this simulation verified the intuitive judgment that using a wider acquisition beam should help reduce the influence of these disturbances. However, once sensor integration time effects were added to the simulation, the intuitive estimates of how varying the acquisition parameters changes the coverage no longer hold true. More in-depth simulations and inclusion of additional terms such as boundary layer effects are needed to further develop this toolkit and make it better suited for acquisition system design studies.

REFERENCES

[1] G. Griseri, 'Silex Mission Overview', presented at the International Workshop on Control of Optical Systems Conference, Breckenridge, CO Feb. 2003.

[2] G. Fletcher, T Hicks, B. Laurent, 'The SILEX Optical Interorbit Link Experiment', Electronics & Communications Engineering Journal, Dec. 1991.

[3] K. Nakagawa, A. Yamamoto, M. Toyoda, 'Performance test result of LUCE (laser utilizing communications equipment) engineering model', Proc. SPIE Vol. 3932, Free-Space Laser Communication Technologies XII, 2000.

[4] M. McCarter, 'Satellite Transformation', Military Information Technology, Vol. 9, No. 4, June 13, 2005.

[5] S. Arnon, N. Kopeika, D. Kedar, A. Zilberman, D. Arbel, A. Livne, M. Guelman, M. Orenstain, H. Michalik, and A.Ginati, 'Performance limitation of laser satellite communication due to vibrations and atmospheric turbulence: Down -link scenario' Intl. Journal of Satellite Communications and Networking , Vo. 21, pp.561-573, (2003)

[6] R. Quaale, C. Hindman, B. Engberg, and P. Collier, 'Mitigating Environmental Effects on Free-Space Laser Communications', IEEE Aerospace Conference, Big Sky, MT 2005

[7] Corda, S., Franz, R. J., Blanton, J.N., Vachon, M. J., and DeBoer, J. B., 'In-Flight Vibration Environment of the NASA F-15B Flight Test Fixture', NASA/TM-2002-210719, 2002.

[8] Schönhoff, U.; Eisenträger, P.; Wandner, K.; Kärcher, H.; Nordmann, R.: End-to-end Simulation of the Image Stability for the Airborne Telescope SOFIA, Astronomical Telescopes and Instrumentation 2000, March 2000, Munich, Germany

[9] Fung, D. E., Doerr, S., and Nunez, M., 'Estimation of Aircraft to Satellite Fade Margin', SAIC Technical Report, April 2004.

[10] S. Lambert and W. Casey, Laser Communications in Space, Artech House, Boston, 1995.

[11] C. Hindman and L. Robertson, 'Beaconless Satellite Laser Acquisition – Modeling and Feasibility', MILCOM 2004 Military Communications Conference, Monterey, CA 2004.

BIOGRAPHY

Dr Charles "Bill" Hindman received his BS degree from the University of Idaho in Mechanical Engineering, his MS degree from the University of Arizona in Mechanical Engineering, and his Ph.D. degree from the University of Colorado at Boulder in Aerospace Engineering. Currently he is the Pointing, Acquisition and Tracking and Laboratory Technical Leads for the multi-user laser communications programs at the Air Force Research Laboratory. His research interests include the modeling, simulation and testing of laser propagation and detection, multi-target tracking, and control systems.

Brian Engberg is an aerospace systems engineer at the Air Force Research Laboratory Space Vehicles Directorate; currently chief systems engineer for the multi-access lasercomm technology branch, developing and integrating relevant technologies into the TSAT space segment. Previous work includes end-to-end small satellite engineering, and systems engineering work on technologies related to large deployable space structures, dynamics and control. Brian holds BS degrees in Aerospace Engineering and Astronomy & Astrophysics from the University of Illinois at Urbana-Champaign, and a MS in Aeronautical & Astronautical Engineering from Stanford.